IMU-based localization and slip estimation for skid-steered mobile robots

Conference Paper · October 2007

DOI: 10.1109/IROS.2007.4399477 · Source: DBLP

4 authors, including:

Jingang Yi
Rutgers, The State University of New Jersey
197 PUBLICATIONS **3,471** CITATIONS

IMU-based Localization and Slip Estimation for Skid-Steered Mobile Robots

Jingang Yi, Junjie Zhang, Dezhen Song, and Suhada Jayasuriya

***Abstract*— Localization and wheel slip estimation of a skid-steered mobile robot is challenging because of the complex wheel/ground interactions and kinematics constraints. In this paper, we present a localization and slip estimation scheme for a skid-steered mobile robot using low-cost inertial measurement units (IMU). We first analyze the kinematics of the skid-steered mobile robot and present a nonlinear Kalman filter (KF)-based simultaneous localization and slip estimation scheme. The KF-based localization design incorporates the wheel slip estimation and utilizes robot velocity constraints and estimates to overcome the large drift resulting from the integration of the IMU acceleration measurements. The estimation methodology is tested and validated experimentally with a computer vision-based localization system.**

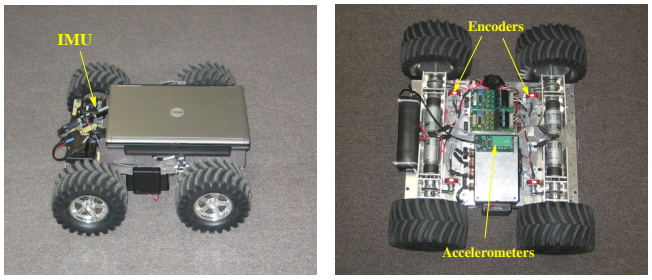

(a) (b)

Fig. 1. A skid-steered four-wheel mobile robot with a sensor suite.

I. Introduction

Skid-steering is a widely used locomotion mechanism for mobile robots. The absence of the steering system of a skid-steered mobile robot, such as the one shown in Fig. 1, makes the robot mechanically robust and simple for outdoor navigation. Due to varying ground surface conditions and wheel/ground interactions, it is challenging to obtain an accurate kinematics and dynamic model for skid-steered mobile robots. Dead-reckoning using wheel encoder measurements or global positioning systems (GPS) are the major techniques to localize a mobile robot. However, the accuracy of the dead-reckoning technique suffers when there is a large wheel slip. For example, for terrain navigation robots, such as Mars Exploration Rovers, large (even 100%) wheel slips have been observed [1]. GPS also suffers signal robustness, availability, and accuracy issues. IMU-based localization can be used for robots. However, such a localization method has to be used combining with other measurements, such as wheel encoders or GPS, to overcome the drifting issue due to the numerical integration of biased measurements.

Wheel slip is typically defined as the ratio of the relative velocity of the wheel contact point and the wheel velocity. Wheel slip plays an important role for not only localization and motion planning but also control of skid-steered robots. For skid-steered mobile robots, lateral velocity along the wheel rotating axis is allowed and the typical zero-velocity nonholonomic constraint for other types of robots, such as unicycle or car-like robots, is no longer valid. If the wheels on each side of a skid-steered robot are running at the same angular velocity, the robot behaves similar to tracked vehicles. Because of this similarity, methods of modeling tracked ground vehicles have been utilized for skid-steered mobile robots. For example, Song *et al.* [2] use the kinematics of tracked vehicles in [3] to estimate wheel slip using a sliding-mode observer design. Because of the difficulty to accurately capture the skid-steering, Anousaki and Kyriakopoulos [4] use an extra wheeled trailer to experimentally study the kinematic relationship for SLAM applications. It is concluded that a kinematic model for an ideal differential-driven wheeled robot cannot be used for skid-steered robots. In [5], a slip-based adaptive trajectory tracking control system is designed for skid-steered robots.

Using inertial devices, such as IMU, to localize a mobile robot has been studied during the last decade. It is well-known that directly integrating acceleration measurements to obtain position information is problematic due to bias or noise measurements in IMU signals. In [6], [7], reduction of the odometry of the skid-steered robots are discussed for dead-reckoning applications using encoder and motor current measurement information. In [8], localization of a tracked vehicle is presented based on kinematic models provided in [9]–[11]. In [12], an IMU-based wheel slip detection scheme is designed for a unicycle-like mobile robot using an extended Kalman filter (EKF) with or without GPS measurements. In [13], [14], velocity constraints, such as zero lateral velocity, are considered to integrate with an EKF or information filter to enhance the localization of the autonomous ground vehicles in the urban area. GPS and wheel encoder measurements are used as input information for the EKF design. Wheel slip is however not considered in the EKF design.

In this paper, we extend the design in [14] to localize skid-steered robots. We present a low-cost IMU-based localization and slip estimation scheme for skid-steered mobile robots. The study in this paper complements the design in [5] to

J. Yi is with the Department of Mechanical Engineering, San Diego State University, San Diego, CA 92182. Email: jgyi@mail.sdsu.edu.

J. Zhang and S. Jayasuriya are with the Department of Mechanical Engineering, Texas A&M University, College Station, TX 77843. Email: {jjzhang,sjayasuriya}@tamu.edu.

D. Song is with the Department of Computer Science, Texas A&M University, College Station, TX 77843. Email: dzsong@cs.tamu.edu.

obtain the wheel slip information using an on-line KF-based estimator and low-cost IMU devices. Based on the robot kinematic models, we consider three velocity constraints and estimates in the robot frame to facilitate the on-line Kalman filter design. The slip estimation is also incorporated into the KF design in real time. The proposed localization and wheel slip estimation methods are experimentally tested and validated using a computer vision-based positioning system.

The contributions of this study are two-folds. First, we incorporate the wheel slip estimation into the robot localization scheme and therefore improve both localization and slip estimation accuracy simultaneously. To our knowledge, most dead-reckoning-based robot localization work do not consider the wheel slip. Second, we present a low-cost IMU-based localization and slip estimation scheme for skid-steered robots. Such an on-line estimation scheme allows us to further develop a slip-based robot control system that can be used in varying ground surface conditions [5].

The remainder of this paper is organized as follows. In section II, we discuss the kinematic modeling of a four-wheel skid-steered mobile robot. Section III presents a nonlinear KF-based localization and slip estimation design. Experimental results are presented in section IV. Finally, we conclude the paper in section V.

II. Skid-Steered Robot Kinematic Models

Fig. 2 shows the kinematic schematic of the skid-steered robot. Without loss of generality, we consider the following modeling assumptions: (1) the mass center of the robot is located at the geometric center of the body frame [1], (2) there is point contact between the wheel and the ground, (3) each side's two wheels rotate at the same speed. and (4) the robot four-wheels are always in contact with the ground surface.

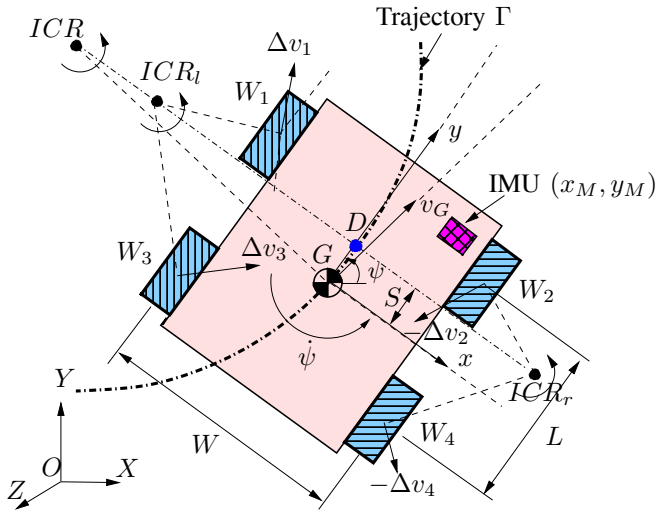

Fig. 2. A kinematic schematic of the skid-steered robot.

Denote the wheel angular velocities ω_i, $i = 1, \cdots, 4$, for front-left, front-right, rear-left, and rear-right wheels, respectively. From the above assumption, we have

$$\omega_1 = \omega_3 = \omega_L, \quad \omega_2 = \omega_4 = \omega_R. \tag{1}$$

Denote the velocities of wheel centers as v_i, $i = 1, \cdots, 4$, for front-left, front-right, rear-left, and rear-right wheels, respectively. The velocity of the robot mass center is denoted by v_G. We define a fixed inertial frame $\mathbf{I}(X, Y, Z)$ and a robot body frame $\mathbf{B}(x, y, z)$ as shown in Fig. 2. The pitch angle (around x-axis), roll angle (around y-axis), and yaw angle (around z-axis) are denoted as θ, ϕ, and ψ, respectively. We also denote the longitudinal and lateral wheel bases as L and W, respectively, as illustrated in Fig. 2.

Given the robot mass center velocity v_G (in the body frame $\mathbf{B}$) and yaw rate $\dot{\psi}$, we calculate the wheel center velocity along the y-axis for left- and right-side's wheels as

$$v_{Ly} = v_{1y} = v_{3y} = v_{Gy} - \frac{W}{2}\dot{\psi}, \tag{2}$$

$$v_{Ry} = v_{2y} = v_{4y} = v_{Gy} + \frac{W}{2}\dot{\psi}. \tag{3}$$

For the IMU located at (x_M, y_M) in the body frame $\mathbf{B}$, we obtain the IMU velocity v_M in the robot body frame $\mathbf{B}$ as

$$v_{Mx} = v_{Gx} - y_M\dot{\psi}, \qquad v_{My} = v_{Gy} + x_M\dot{\psi}. \tag{4}$$

We define the longitudinal wheel slips λ_i as

$$\lambda_i = \frac{r\omega_i - v_{iy}}{r\omega_i} = -\frac{\Delta v_{iy}}{r\omega_i}, \quad i = 1, \ldots, 4, \tag{5}$$

where r is the effective wheel radius and $\Delta v_{iy} = v_{iy} - r\omega_i$. For left- and right-side's wheels, the wheel slips satisfy

$$\lambda_L = \lambda_1 = \lambda_3, \quad \lambda_R = \lambda_2 = \lambda_4$$

due to the robot operating assumption. It is also observed that wheel slip $\lambda \in [0, 1]$ if the wheel is under traction and $\lambda \in (-\infty, 0]$ if the wheel is under braking. In order to constrain the slip calculation within the magnitude of one, using the same treatment as in [9], we take $\lambda = -1$ if $\lambda < -1$ under the braking case. Therefore, we consider the wheel slip $\lambda \in [-1, 1]$.

We denote the instantaneous center of rotation (ICR) of the left-side wheel contact points, right-side wheel contact points, and the robot body as ICR_l, ICR_r, and ICR_G, respectively. It is known that ICR_l, ICR_r and ICR_G lie on a line parallel to the x-axis [8], [11], [15]. We denote the x-y coordinates for ICR_l, ICR_r, and ICR_G as (x_l, y_l), (x_r, y_r), and (x_G, y_G), respectively. We find that the y-coordinate S of the ICRs satisfies the following constraints [8], [15].

$$S = y_l = y_r = y_G = \frac{v_{Gx}}{\dot{\psi}}. \tag{6}$$

It is straightforward to calculate the transformation relationship from the body frame $\mathbf{B}$ to the inertial frame $\mathbf{I}$ given by the following orthonormal matrix.

$$C_B^I = \begin{bmatrix} c_\theta c_\psi & -s_\psi c_\phi + c_\psi s_\phi s_\theta & s_\phi s_\psi + c_\psi s_\theta c_\phi \\ c_\theta s_\psi & c_\phi c_\psi + s_\theta s_\phi s_\psi & -s_\phi c_\psi + s_\theta c_\phi s_\psi \\ -s_\theta & c_\theta s_\phi & c_\phi c_\theta \end{bmatrix}, \tag{7}$$

[1] Similar results could be obtained if the mass center of the robot is located differently with the robot geometric center.

where $c_\theta = \cos\theta$, $s_\theta = \sin\theta$, and the same notation for other angles ϕ and ψ.

Let us denote the position and velocity vectors of the IMU in the inertial frame $\mathbf{I}$ as $\mathbf{P}_I \in \mathbb{R}^3$ and $\mathbf{V}_I \in \mathbb{R}^3$, respectively. Denote the measured acceleration in the body frame $\mathbf{B}$ by the IMU as $\mathbf{A}_B \in \mathbb{R}^3$. We obtain the following kinematic motion equations for the IMU on the robot.

$$\dot{\mathbf{P}}_I = \mathbf{V}_I. \tag{8a}$$

$$\dot{\mathbf{V}}_I = C_B^I(\mathbf{A}_B + \mathbf{w}_1) + \mathbf{G}, \tag{8b}$$

where $\mathbf{G} = [0 \;\; 0 \;\; -g]^T$, g is the gravitational constant, and $\mathbf{w}_1 = [w_{ax} \; w_{ay} \; w_{az}]^T$ is the IMU measurement noise along x, y, and z axes, respectively.

The kinematic models given by Eqs. (8a) and (8b) describe the relationship between position vector $\mathbf{P}_I$ and velocity vector $\mathbf{V}_I$ in the inertial frame $\mathbf{I}$, and acceleration measurements $\mathbf{A}_B$ in the body frame $\mathbf{B}$. In the next section, we discuss how to obtain the velocity estimates and motion constraints and KF design.

III. Constrained Kalman Filter Design

A. Velocity estimates and constraints

We consider the robot velocity estimates and constraints in the body frame $\mathbf{B}$. Since the robot's four wheels are always in contact with the ground, it is straightforward to obtain the following velocity constraint for the IMU device in the z direction.

$$v_{Mz} = 0. \tag{9}$$

For the IMU longitudinal velocity v_{My}, we obtain an estimate as follows. Using the definition of the slip in Eq. (5), we have $v_{Ly} = v_{1y} = v_{3y} = (1-\lambda_L)r\omega_L$, $v_{Ry} = v_{2y} = v_{4y} = (1-\lambda_R)r\omega_R$. From Eqs. (2)-(4), we obtain

$$v_{My} = \frac{r}{2}\left[(\omega_L + \omega_R) - (\lambda_L\omega_L + \lambda_R\omega_R)\right] + x_M\dot{\psi}. \tag{10}$$

Using the wheel encoder reading and the slip estimation, we calculate the IMU longitudinal velocity in the body frame v_{My} by Eq. (10). Since the calculation of wheel slips λ_L and λ_R is dependent on the values of the wheel translational velocity estimates, we need to enforce a bound on slips λ_L and λ_R in Eq. (10) to ensure a stable KF design.

Notice that if $\omega_L \le \omega_R$, the robot turns left and the wheel slips satisfy $\lambda_L \le 0$ and $\lambda_R \ge 0$ due to the robot kinematics. Similarly, we obtain that if $\omega_L > \omega_R$, then $\lambda_L > 0$ and $\lambda_R < 0$. Therefore, we modify Eq. (10) as

$$v_{My} = \frac{r}{2}\left[(\omega_L + \omega_R) - (\lambda'_L\omega_L + \lambda'_R\omega_R)\right] + x_M\dot{\psi}, \tag{11}$$

where

$$\lambda'_L(\lambda'_R) = \begin{cases} \max\{\lambda_L(\lambda_R), 0\} & \text{if } \omega_L \ge \omega_R \; (\omega_L \le \omega_R) \\ \min\{\lambda_L(\lambda_R), 0\} & \text{if } \omega_L < \omega_R \; (\omega_L > \omega_R). \end{cases}$$

For the lateral velocity v_{Mx}, from Eqs. (4) and (6), we obtain

$$v_{Mx} = (S - y_M)\dot{\psi}. \tag{12}$$

In order to estimate the lateral velocity, we have to estimate the y-axis coordinate S of the instantaneous rotation centers.

First, we consider the dependency of S on ground surface conditions. Fig. 3(a) shows robot trajectories on three different ground surfaces, namely, concrete, tile, and sand, with constant wheel velocities $\omega_L/\omega_R = 140/60$ rpms. Fig. 3(b) shows the calculated values of S on these three ground surfaces. It is observed that the value of S does not change significantly due to different ground surface conditions. Therefore, the value of S is considered independent of the ground conditions.

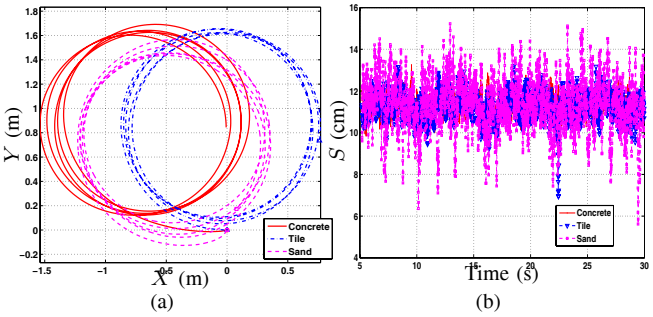

(a) (b)

Fig. 3. (a) Robot trajectories with $\omega_L = 140$ rpm and $\omega_R = 60$ rpm on three different ground surfaces and (b) calculated values of S.

We then estimate the value of S on the same ground condition with various wheel velocity combinations. To facilitate the discussion, we introduce a non-dimensional variable γ as the ratio of difference and sum of left- and right-side's wheel angular velocities, namely,

$$\gamma = \frac{\omega_L - \omega_R}{\omega_L + \omega_R} = \frac{1-\lambda_\omega}{1+\lambda_\omega},$$

where $\lambda_\omega = \frac{\omega_R}{\omega_L}$ is the ratio of right and left sides' wheel angular velocities. The value of S is considered as a function of variable γ. If $\omega_L = \omega_R$, $\gamma = 0$ and S is a finite value due to the non-zero lateral velocity of mass center G [8]. If $\omega_L = -\omega_R$, $\gamma \to \infty$ and $S = 0$ since the robot is rotating about G without any translational motion. Therefore, we approximate the function $S(\gamma)$ as

$$S(\gamma) = \frac{a_1}{a_2\gamma + a_3}, \tag{13}$$

where the coefficients a_i, $i = 1, 2, 3$, are determined by curve-fitting the experimental data.

We have run several experiments with various wheel velocity combinations (we choose $\omega_L \ge \omega_R$ so that $\gamma \ge 0$) on both concrete and sand road surfaces. We calculate S using the computer vision-based localization system (we will describe the experiments in Section IV-A). Fig. 4 shows the experimental data and the data-fitted curve. Numerical values of parameters $a_1 = 5.39$ cm, $a_2 = 0.77$, and $a_3 = 0.16$ are obtained using a nonlinear least-square algorithm for the function given in Eq. (13). Note that if $\gamma < 0$, i.e., $\omega_L < \omega_R$, we can take a similar S curve as shown in Fig. 4. We use $S(\gamma)$ given in Eq. (13) to approximate the estimate of the lateral velocity v_{Mx} in Eq. (12).

With the IMU velocity constraints and estimates given by Eqs. (9), (11) and (12), we are now ready to design a KF-based localization and slip estimation scheme.

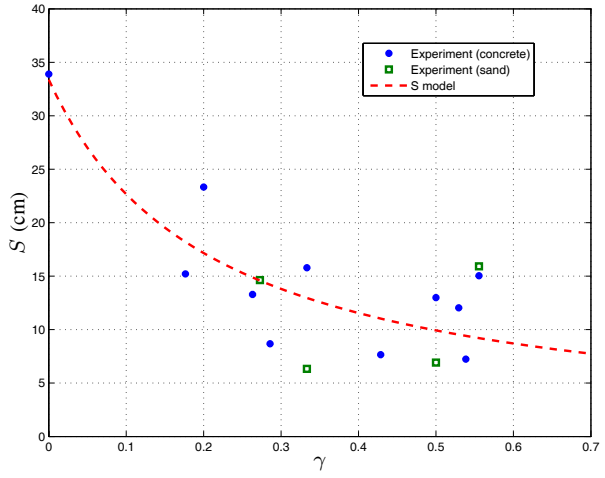

Fig. 4. Experimental data (through computer vision-based localization) and data-fitted curve by Eq. (13) for variable S.

B. Nonlinear Kalman filter design

We obtain an estimate of pitch, roll, and yaw angles by directly integrating the accurate angular rate measurements from the IMU. Therefore, we assume that we know these attitude angles and the transformation matrix C_B^I given in Eq. (7) is then calculated.

We consider the IMU velocity $\mathbf{V}_B$ in the body frame as the measurement vector $\mathbf{z}$ for the KF design, namely,

$$\mathbf{z} = \mathbf{V}_B = \begin{bmatrix} v_{Mx} \\ v_{My} \\ v_{Mz} \end{bmatrix} = (C_B^I)^T \mathbf{V}_I. \tag{14}$$

Here $\mathbf{z}$ is obtained using Eqs. (12), (11) and (9). Considering the measurement noise and ground topography, we modify Eq. (14) as

$$\mathbf{z} = \mathbf{V}_B + \mathbf{w}_2, \tag{15}$$

where $\mathbf{w}_2$ represents the estimation and constraint variations that are defined later in this section. We define a state variable $\mathbf{X} = [\mathbf{P}_I \ \mathbf{V}_I]^T \in \mathbb{R}^6$ and re-write the motion equations (8) and (15) in a discrete-time form according to the IMU data sampling period as

$$\mathbf{X}(k+1) = F(k)\mathbf{X}(k) + B(k)\mathbf{A}_B(k) + B(k)\mathbf{w}_1(k) \tag{16a}$$

$$\mathbf{z}(k) = H(k)\mathbf{X}(k) + \mathbf{w}_2(k), \tag{16b}$$

where

$$F(k) = \begin{bmatrix} \mathbf{I}_3 & \Delta T \mathbf{I}_3 \\ \mathbf{0}_{3\times 3} & \mathbf{I}_3 \end{bmatrix}, \ B(k) = \begin{bmatrix} \mathbf{0}_{3\times 3} \\ \Delta T C_B^I(k) \end{bmatrix},$$
$$H(k) = \begin{bmatrix} \mathbf{0}_{3\times 3} & \left(C_B^I(k)\right)^T \end{bmatrix},$$

$\mathbf{I}_n$ is the $n \times n$ identity matrix, and ΔT is the IMU data-sampling period.

We assume that measurements noise $\mathbf{w}_1$ and $\mathbf{w}_2$ are independent and white, i.e. $\mathbf{w}_1 \sim \mathcal{N}(0, Q)$, and $\mathbf{w}_2 \sim \mathcal{N}(0, R)$. The covariance matrix $Q = \text{diag}(\sigma_{ax}^2, \sigma_{ay}^2, \sigma_{az}^2) \in \mathbb{R}^{3\times 3}$ denotes the acceleration measurements noise along the x-y-z axis. For the covariance matrix $R = \text{diag}(\sigma_{z1}^2, \sigma_{z2}^2, \sigma_{z3}^2) \in \mathbb{R}^{3\times 3}$, σ_{z1}^2 is the variance for the lateral velocity estimate v_{Mx} in Eq. (12). $\sigma_{z2}^2 = r^2\sigma_{en}^2 + x_M^2\sigma_{\dot{\psi}}^2$ is the variance for the longitudinal velocity v_{My} estimate in Eq. (11), where σ_{en}^2 is the variance for the wheel encoder measurement and $\sigma_{\dot{\psi}}^2$ is the variance for the yaw rate measurement, respectively. σ_{z3}^2 is the variance for the ground surface topography.

The Kalman filter implementation for the above systems given by Eq. (16) can be written as a prediction step ($\hat{\mathbf{X}}(k|k-1)$) and a correction step ($\hat{\mathbf{X}}(k|k)$) recursively as follows.

$$\hat{\mathbf{X}}(k|k-1) = F(k)\hat{\mathbf{X}}(k-1|k-1) + B(k)\mathbf{A}_B(k) \tag{17a}$$

$$P(k|k-1) = F(k)P(k|k-1)F^T(k) + B(k)QB^T(k) \tag{17b}$$

$$\hat{\mathbf{X}}(k|k) = \hat{\mathbf{X}}(k|k-1) + W(k)\left[\mathbf{z}(k) - H(k)\hat{\mathbf{X}}(k|k-1)\right] \tag{17c}$$

$$W(k) = P(k|k-1)H^T(k)S^{-1}(k) \tag{17d}$$

$$S(k) = H(k)P(k|k-1)H^T(k) + R \tag{17e}$$

$$P(k|k) = (\mathbf{I}_6 - W(k)H(k))P(k|k-1)(\mathbf{I}_6 - W(k)H(k))^T + W(k)RW^T(k). \tag{17f}$$

The above KF estimation design is not linear in the state variable $\mathbf{X}(k)$. The velocity estimate $\mathbf{V}_I$ at the kth step is used to calculate wheel slips λ_L' and λ_R' (Eq. (11)) at the $(k+1)$th step for KF measurement update. Since wheel slip calculation is highly nonlinear in IMU velocity $\mathbf{V}_B = (C_B^I)^T\mathbf{V}_I$, the KF design is indeed a nonlinear system in the state variable $\mathbf{V}_I$. We have experimentally noticed that if we use the non-constrained slip calculation for longitudinal velocity v_{My} in Eq. (10) instead of the constrained one in Eq. (11), the output of KF estimation is unstable due to such a nonlinear feedback of wheel slip calculation. The stability issue of the nonlinear KF design is currently under investigation.

We have also noticed that the accuracy of the $S(\gamma)$ estimate is secondary compared with the importance of introducing such a velocity estimate as one KF measurement in Eq. (14). For example, if the robot is running at the same wheel velocity, the output trajectory of the KF design using only longitudinal and vertical velocity estimates and constraints is not satisfactory due to the noise in the low-cost IMU devices. Adding a lateral velocity estimate given by Eqs. (12) and (13) into $\mathbf{z}$ of the KF design significantly increases the KF output accuracy.

IV. Experiments

A. Experimental systems

We have built an on-board sensor suite on the skid-steered mobile robot shown in Fig. 1. We use a low-cost IMU from Microstrain Inc. for attitude measurements and a 3-axis accelerator from Sentera Technology Inc. The optical wheel encoder reading and four-wheel motion control are implemented on a real-time system from Acroname Robotic Inc. The control system is a two-level hierarchy: the control

algorithm and Kalman filter design are located in the on-board laptop system and the PID-based motor control is located at the low-level real-time system.

The attitude information is obtained through the integration of the angular rate measurements from IMU at a frequency of 100 Hz. The encoder reading is obtained at a frequency of 4 Hz. The KF-based localization and slip estimation scheme is updated at a frequency of 125 Hz. The PID motion control algorithm is updated at 16 Hz. A computer vision-based localization system is employed to provide the robot's absolute position information in all experiments. The output of the computer-based localization system is taken as a benchmark to compare and validate the proposed localization and slip estimation scheme.

B. Experimental results

Fig. 5 shows the comparison results of the robot localization under three different implementation schemes when the robot is under a wheel velocity combination of $\omega_L = 120$ rpm and $\omega_R = 60$ rpm.

Here we do not compare the results with the localization information by directly integrating the acceleration measurements since such an integration results drift significantly away from the true trajectory. Instead, we compare the KF-based localization schemes using three different sets of measurements respectively. These measurement sets are: (1) the vertical velocity v_{Mz} constraint given by Eq. (9) and the longitudinal velocity estimate *without* considering the wheel slip, (2) both the vertical velocity constraint and longitudinal velocity estimate *with* the wheel slip feedback, i.e., Eq. (11), and (3) all three-dimensional velocity constraints and estimates with the wheel slip feedback. From Fig. 5, we observe that the first scheme has a large error (black-triangular line). By considering the wheel slip estimation, the localization results improve significantly (dash and dash-dot lines in Fig. 5) and the estimated trajectories are close to the true trajectory.

Fig. 6 shows the robot velocities in the body frame $\mathbf{B}$ and the localization errors. Again, we consider the KF design under the aforementioned three cases. Fig. 6(a) shows the localization errors and Fig. 6(b) shows the estimated velocity comparisons with the vision-based results. Using three-dimensional velocity constraints and estimates and incorporating wheel slip estimation into the KF design reduce the localization error significantly (Fig. 6(a)). The estimated velocities in such a scheme are close to their true values (Fig. 6(b)). The cyclic pattern of the localization errors shown in Fig. 6(a) comes from the data-recording timing difference between the vision and on-board IMU systems. We believe such a system error can be further reduced by synchronizing the vision and on-board computer systems.

We also compare the KF-based slip estimation under various wheel angular velocity combinations. Figs. 7(a) and 7(b) show the slip estimations for the wheel velocity combinations $\omega_L/\omega_R = 140/40$ and $120/80$ rpms, respectively. We plot the computer vision-based slip information in each case for comparison purposes. We choose these wheel

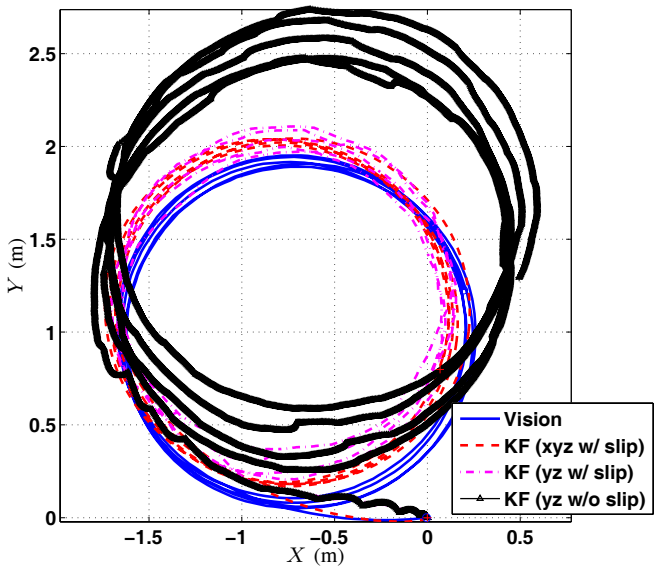

Fig. 5. KF-based XY trajectory estimation using (a) xyz velocity constraints and estimates with the wheel slip consideration, (b) yz velocity constraints and estimates with the wheel slip consideration, and (c) yz velocity constraints and estimates without the wheel slip consideration.

velocity combinations because such combinations represent a decreasing wheel slip trend. For example, if the robot runs at $\omega_L/\omega_R = 120/80$, then wheel slips are smaller (Fig. 7(b)) than those at $\omega_L/\omega_R = 140/40$ (Fig. 7(a)) since the robot needs a small traction force to overcome the wheel resistance at a larger radius turn. The slip estimation results shown in Figs. 7(a) and 7(b) clearly demonstrate such a decreasing trend and the IMU-based slip estimates match the vision-based slip calculation very well.

V. Conclusion

Skid-steered mobile robots are used widely for robotic navigation applications. Modeling and localization of skid-steered robots are challenging due to the complex robot dynamics and wheel/ground interactions. In this paper, we present a nonlinear KF-based simultaneous localization and slip estimation scheme for skid-steered robots. The proposed localization and slip estimation scheme uses only the on-board low-cost IMU devices and wheel encoder measurements. Comparing with the dead-reckoning-based localization approach, we incorporate the wheel slip information as feedback measurements into the KF design and therefore improve the accuracy of both localization and slip estimation. Moreover, we fully utilize the robot lateral velocity information in the KF design by taking advantage of the kinematic modeling of skid-steered robots. Such a treatment further improves the estimation accuracy. The localization and slip estimation design is tested and validated experimentally with a computer vision-based positioning system. Integration of the slip estimation scheme with the slip-based robot controller is also under the current development and we will report the new developments in the near future.

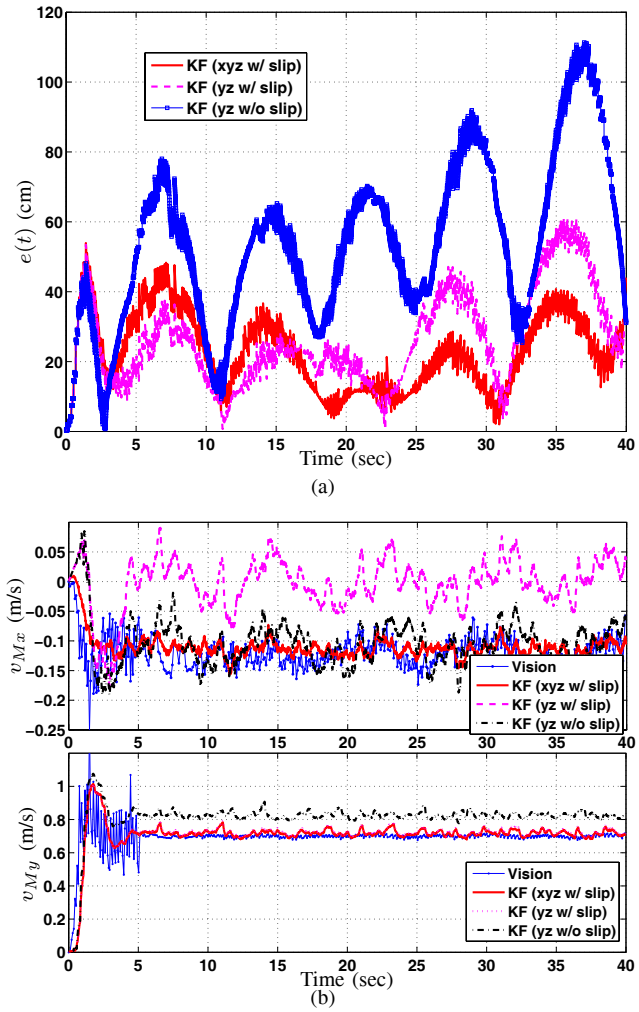

Fig. 6. (a) Localization errors (compared with vision-based localization) and (b) KF-based x and y velocities using various kinematics constraints and estimations.

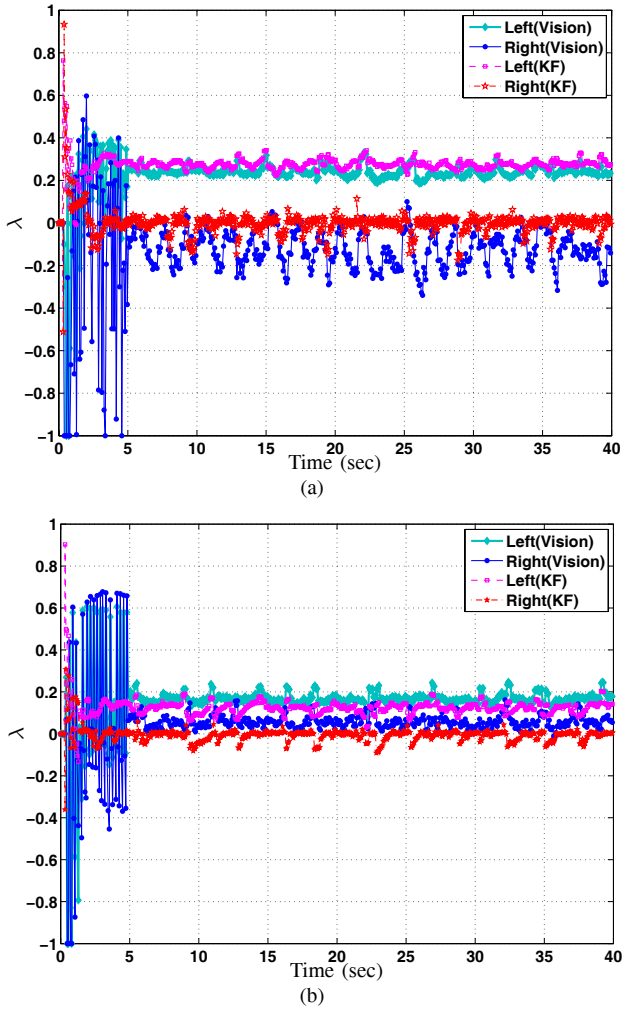

Fig. 7. Estimated wheel slip information using KF-based and computer vision-based localization schemes under various wheel velocity combinations. (a) $\omega_L/\omega_R = 140/40$ rpms and (b) $\omega_L/\omega_R = 120/80$ rpms.

ACKNOWLEDGMENT

The authors thank Brandon Green, Diyogu Maithripala, Chang Young Kim, Yiliang Xu, Zane Goodwin, and Dr. Paolo Bernasconi for their help and discussions.

REFERENCES

[1] A. Angelova, L. Matthies, D. Helmick, and P. Perona, "Slip Prediction Using Visual Information," in *Proc. Robotics: Sci. Sys.*, Philadelphia, PA, 2006.

[2] Z. Song, Y. Zweiri, L. Seneviratne, and K. Althoefer, "Nonlinear Observer for Slip Estimation of Skid-Steering Vehicles," in *Proc. IEEE Int. Conf. Robotics Automation*, Orlando, FL, 2006, pp. 1499–1504.

[3] A. Le, D. Rye, and H. Durrant-Whyte, "Estimation of Track-Soil Interactions for Autonomous Tracked Vehicles," in *Proc. IEEE Int. Conf. Robotics Automation*, Albuquerque, NM, 1997, pp. 1388–1393.

[4] G. Anousaki and K. Kyriakopoulos, "A Dead-Reckoning Scheme for Skid-Steered Vehicles in Outdoor Environments," in *Proc. IEEE Int. Conf. Robotics Automation*, New Orleans, LA, 2004, pp. 580–585.

[5] J. Yi, D. Song, J. Zhang, and Z. Goodwin, "Adaptive Trajectory Tracking Control of Skid-Steered Mobile Robots," in *Proc. IEEE Int. Conf. Robotics Automation*, Roma, Italy, 2007, pp. 2605–2610.

[6] L. Ojeda and J. Borenstein, "Methods for the Reduction of Odometry Errors in Over-Constrained Mobile Robots," *Autonomous Robots*, vol. 16, no. 3, pp. 273–286, 2004.

[7] L. Ojeda, D. Cruz, G. Reina, and J. Borenstein, "Current-Based Slippage Detection and Odometry Correction for Mobile Robots and Planetary Rovers," *IEEE Trans. Robotics*, vol. 22, no. 2, pp. 366–378, 2006.

[8] J. Martinez, A. Mandow, J. Morales, S. Pedraza, and A. Garcia-Cerezo, "Approximating Kinematics for Tracked Mobile Robots," *Int. J. Robot. Res.*, vol. 24, no. 10, pp. 867–878, 2005.

[9] M. Kitano and M. Kuma, "An Analysis of Horizontal Plane Motion of Tracked Vehicles," *J. Terramechanics*, vol. 14, no. 4, pp. 211–225, 1977.

[10] J. Wong, *Theory of Ground Vehicles*, 3rd ed. Hoboken, NJ: John Wiley & Sons, Inc., 2001.

[11] J. Wong and C. Chiang, "A General Theory for Skid Steering of Tracked Vehicles on Firm Ground," *Proc. Inst. Mech. Eng., Part D: J. Auto. Eng.*, vol. 215, pp. 343–355, 2001.

[12] C. Ward and K. Iagnemma, "Model-Based Wheel Slip Detection for Outdoor Mobile Robots," in *Proc. IEEE Int. Conf. Robotics Automation*, Roma, Italy, 2007, pp. 2724–2729.

[13] S. Sukkarieh, "Low Cost, High Integrity Aided Inertial Navigation Systems for Land Vehicle Applications," Ph.D. dissertation, Dept. Mech. Mechatro. Eng., Univ. Sydney, Austrialia, 2000.

[14] G. Dissanayake, S. Sukkarieh, E. Nebot, and H. Durrant-Whyte, "The Aiding of a Low-Cost Strapdown Inertial Measurement Unit Using Vehicle Model Constraints for Land Vehicle Applications," *IEEE Trans. Robot. Automat.*, vol. 17, no. 5, pp. 731–747, 2001.

[15] K. Weiss, "Skid-Steering," *Auto. Eng.*, pp. 22–25, 1971.